JOURNAL OF COMMUNICATION AND INFORMATION SYSTEMS, VOL. 35, NO.1, 2020.

357

# Propagation Models for 5G Signals in the 60 GHz Band

Gustavo K. Marengo, Eduardo S. Lima, Gabriel E. S. Leite, Arismar C. S. Junior and Luciano L. Mendes

*Abstract*—The millimeter wave frequency band is a fundamental resource for the emerging 5G mobile communication systems in order to increase the mobile data capacity. The unlicensed 60 GHz band will play an important role for the high data rate mobile networks and accurate propagation channel models are necessary for efficiently designing the physical and link layers of the future systems. The aim of this paper is to present the main propagation models and scenarios that can be used to estimate the impact of the communication channel in 5G signals operating in 60 GHz bands, highlighting the challenges and advantages of exploiting this frequency band. An overview of 5G channel models for 60 GHz and a path-loss comparison among them for a urban microcell with line-of-sight (UMi-LOS) environment are also presented in this paper.

*Index Terms*—5G Networks, 60 GHz, Millimeter Waves, Prediction Models, Propagation Environments.

## I. INTRODUCTION

The Fifth Generation of Mobile Network (5G) encompasses four main application scenarios: massive Machine Type Communications (mMTC), enhanced Mobile Broadband (eMBB), Ultra Reliable Low Latency Communications (URLLC) communications [1] and enhanced Remote Area Communications (eRAC) [2]. Particularly for the eMBB scenario, the use of Millimeter Wave (mm-wave) has been highlighted as a key enabler to address the 5G requirements [3] [4]. Nowadays, the majority of countries exploit the sub-6GHz bands for the current mobile networks [5]. The available spectrum for 5G services in the sub 6 GHz is not enough to address all requirements defined for 5G networks [6]. Hence, the use of higher frequencies bands in the mm-wave bands is necessary for the 5G networks to unleash its full potential to the market. The 60 GHz band is receiving a lot of attention because of the large unlicensed bandwidth that can be exploited by the mobile operators [7].

The main advantages of exploiting the mm-wave bands at 60 GHz is the in the available bandwidth and, consequently, the higher throughput that can be delivered to the users [8]. However, there are some procedures which should be take into account to ensure the system efficiency and stability, since this band presents high path loss, requiring complex solutions for increasing the range and reliability. One way to evaluate the

G. k. Marengo, E. S. Lima, G. E. S. Leite, L. Leonel Mendes, and A. Cerqueira S. Jr are with the Inatel, Santa Rita do Sapucaí, MG 37400-000, Brazil (e-mails:gustavo.kmarengo@gmail.com, lucianol@inatel.br).

predict the network operation is by using channel models and prediction models for the mm-wave bands. A channel model is a representation of the environment scenario between transmitter and receiver, including the features and peculiarities that affect the received power. A prediction model is a tool to estimate signal power levels at the receiver, taking the operational parameters of the link into account [9]. Such models are used to simulate and reproduce the propagation channel in a cost-effective approach, with the purpose of accurately reproduce the behaviour of the channel. The channel models are typically compared with field measurements to evaluate its accuracy and limitations. There are several ongoing campaign targeting 5G channel measurements and modeling, such as Wireless World Initiative New Radio (WINNER) [10], European Cooperation in Science and Technology (COST) 2100 [11], Mobile and wireless communications Enablers for the Twenty-twenty Information Society (METIS) [12] and New York University Simulator (NYUSIM) [13] [14]. The 3rd Generation Partnership Project (3GPP) TR 38.901 model is an extension of the 3GPP TR 38.900 models to include frequencies up to 100 GHz. The new models supports urban macrocell (UMa), urban microcell (UMi) and indoor scenarios [15]. Additionally, Andrews et.al in [16] reported a mm-wave overview of analytical techniques and mathematical models for mobile systems. These recent contributions show the relevance of accurate channel models for the development of future wireless communication systems.

Several propagation characteristics, besides Free Space Path Loss (FSPL), impair the wireless communication in the mm-wave band. For instance, in higher frequencies, the small wavelength of the signal results in a interaction between the signal and elements in the atmosphere, such as water vapor and rain droplets. In this case, this interactions affects the overall path loss, depending on the size and shape of raindrops and rain rate. Additionally, high penetration losses of signals from outdoors to indoor environments severely reduce the received power level of signals at the mm-wave signals and limits the covered area. The penetration losses in mm-wave for several materials have been reported in [15], where the authors demonstrated 24.4 dB and 45.1 dB attenuation, for a mm-wave signal penetrating through two walls and four doors, respectively [17]. In addition, part of the energy also suffers reflections, diffuse scattering and diffraction, resulting in a considerable impact on mm-wave propagation [18]. For mm-wave in higher frequencies, above 40 GHz, the reduced size of the wavelength stats to interact with the molecules of the gases that compose the atmosphere. Gases that resonates at the frequency of the mm-wave signal can absorb the energy of

the electromagnetic wave [19], reducing the power level at the receiver. In this context, the main absorbing gases at mm-wave frequencies below 100 GHz are the water vapor ($H_2O$) and the oxygen ($O_2$). Other import aspect is the foliage attenuation, due to vegetation between the transmitters and receivers [20]. The human blockage also plays an important role, since the human body can introduce high attenuation at the mm-wave bands [21]. According with [22], the human body attenuation can achieve looses up to 25 dB for a single person. Despite these propagation characteristics, several techniques have been proposed to overcame these issues, such as antenna arrays, beamforming and Multiple-Input Multiple-Output (MIMO) [23].

Massive MIMO is an interesting tool to mitigate the high FSPL at mm-wave bands. The directive gains provided by the beamforming techniques with large number of antennas can compensate the attenuation introduced by the channel. Massive MIMO also can be used to improve the mm-wave spectrum efficiency. The main drawback of the mm-wave radio is the complexity of the Radio Frequency (RF) front-end. Due to the high cost and high power consumption of the devices in mm-wave band, the analog RF processing has been emerging as a potential solution. Analog beamforming techniques relies on controlling the phase of each transmitted signal by the antenna array using analog phase shifter circuit [24]. Channel estimation is another important challenge in MIMO in mm-wave bands, mainly when multiple users are sharing the time-frequency-space resources. Compressed channel estimation is a promising solution for improving the analog beamforming performance [25]. From the practical implementation, power-consumption of the Analog to Digital Converter (ADC) and Digital to Analog Converter (DAC) is another barrier that needs to be overcome. Advances in low-power consumption and low-cost Complementary Metal-Oxide-Semiconductor (CMOS) for ADC and DAC converters have enabled high-frequency chips for commercial mobile devices [26]. In addition, expressive advances have been achieved in power amplifiers and adaptive array combing, which make the mm-wave frequency range feasible for 5G networks [27].

This tutorial discusses the propagation models and related environments with focus in the 60 GHz band. In this context, we have investigated five main types of environments. The first one considers the propagation in a free-space scenario. The second one considers a rainy environment, in which the rain drop causes a significant attenuation in mm-wave band. The third scenario considers an urban environment with different types of obstacles, such as: buildings, houses, vehicles, human beings and lamp posts. The fourth environment considers vegetation with trees, bushes, lakes and rivers. Finally, the last one considers an environment with the main suspense particles. For 60 GHz band, the attenuation caused by obstacles and by environments with suspended particles is considerable [14]. Also, this tutorial describes the models for the propagation scenarios and prediction models to estimate attenuation introduced by the communication channel. The propagation scenario models are: COST 2100, 3GPP TR 38.901, METIS, NYUSIM, Fifth Generation of Channel Model (5GCM) and

Millimetre-Wave Based Mobile Radio Access Network for Fifth Generation Integrated Communications (mmMAGIC). The prediction models are: Alpha, Beta and Gamma (ABG) model, Close-in (CI) free space propagation models and Close-in Free Space Propagation Path Loss with a Frequency-Weighted Exponent (CIF) models [28]. Finally, the paper brings an overview of 5G channel models for 60 GHz and a path-loss comparison among them for a UMi Line-of-Sight (LOS) environment.

This tutorial is structured as follows: Section II presents the main characteristics of 60 GHz band and describes the channel models parameters. Section III introduces the propagation scenario models for the 5G signals. Section IV describes the prediction models for millimeter-wave signals. Section V compares the prediction models with field measurements, while Section VI explains the relationship between prediction models and propagation scenario models. Finally, Section VII brings the main conclusions of the paper.

## II. THE 60 GHz BAND - PRINCIPLES, FEATURES AND CHANNEL PROPAGATION SCENARIOS

The 60 GHz band is an unlicensed band located in the Extremely High Frequency (EHF) spectrum, also known as the mm-wave range. It provides a huge amount of bandwidth for high data rates communication systems [5] [29]. The main drawback of systems operating in the 60 GHz frequency range is the high attenuation introduced by the channel [30] [31]. Typically, applications at 60 GHz might are related with indoor communication links [32]. For instance, several works have reported the 60 GHz usage for Wireless Personal Area Network (WPAN) and Wireless Local Area Network (WLAN) [30] [33]. Although the 60 GHz band presents high attenuation, its use for outdoor communication links is being considered in the future mobile networks [34]. Several countries around the world have specified the 60 GHz frequency band for mobile communication, as reported in Table I, with bandwidths raging from 3.5 GHz to 9 GHz [30] [35]. Hence, the 60 GHz bands can provide the high bandwidth and throughput required by several applications foreseen for 5G and beyond 5G networks.

TABLE I
BANDWIDTH ALLOCATION IN 60 GHz BAND FOR 5G SERVICES AROUND THE WORLD [30].

| Regions | Freq. Band | Bandwidth |
|---------|------------|-----------|
| U.S.A | 57 GHz - 64 GHz | 7 GHz |
| Canada | 57 GHz - 64 GHz | 7 GHz |
| Australia | 59.4 GHz - 62.9 GHz | 3.5 GHz |
| Japan | 59 GHz - 66 GHz | 7 GHz |
| Europe | 57 GHz - 66 GHz | 9 GHz |

Europe has defined the largest bandwidth for 5G operation in the 60 GHz band, where up to 9 GHz can be employed for mobile services. Typically, this band is divided in chunks of 2 GHz that can be accessed by a single user [35]. For instance, a 2-GHz bandwidth transmission employing Quadrature Phase Shift Keying (QPSK), 16-Quadrature Amplitude Modulation (QAM) and 64-QAM results in throughput of 4 Gbit/s, 6 Gbit/s and 8 Gbit/s, respectively. Although the focus on using 60 GHz is mobile network, such frequency range has also been used

in Inter-Vehicle Communication (IVC) system, demonstrating 1 Mbit/s throughput between two running vehicles [36].

Several propagation characteristics impair the mm-wave communication, leading to a need for accurate propagation channel models. A channel is defined by the physical environment in which the electromagnetic signal propagates from a transmitter to a receiver. The next subsections will describe the main impairments introduced by the channel.

## A. Free Space

Before discussing the electromagnetic wave propagation mechanisms in different channel models, it is necessary to consider the FSPL [37] [38].

Fig. 1 shows the radiation pattern from a isotropic antenna, represented by a sphere with the same power density at all points on the edge of the sphere. Since the receiving antenna has a finite effective area, it captures only a parcel of the radiated energy, resulting in the free space attenuation. The size of this sphere increases with the square of the distance and the effective area of the antennas reduces with the square of the frequency, meaning that the free space attenuation increases with distance and frequency. If the transmit and receive antennas are directive, the receive power assuming perfect alignment of the antennas is given by [38]

$$P_r = G_r G_t \left( \frac{\lambda}{4\pi D} \right)^2 P_t, \tag{1}$$

where $G_t$ and $G_r$ are the transmit and receive antennas gains, respectively, $D$ is the distance between the receiving and transmit points, and $\lambda = c/f$ is the wavelength with $c$ being the phase speed of the wave.

It is important to highlight that the antenna gains are defined by the operation frequency and by design constraints, such as weight, dimensions, and cost. Eq. 2 represents the Eq. 1 in logarithmic scale [38]

$$P_r \,[\text{dBm}] = P_t \,[\text{dBm}] + G_t \,[\text{dB}] + G_r \,[\text{dB}] - L \,[\text{dB}], \tag{2}$$

The path loss $L$ (dB) represents the attenuation due to the FSPL and is given by

$$L = 32.44 + 20 \log (f \,[\text{MHz}]) + 20 \log (D \,[\text{km}]) \tag{3}$$

The free space is a theoretical model, which represents a signal propagation throughout a scenario without obstacles and environment losses. Assuming 10 km between transmitter and receiver, operating at 60 GHz, the attenuation is approximately 148 dB, considering only the path loss, without environmental effects. However, the channel models must consider such environmental effects for providing a better received power estimation, since a real propagation scenario presents obstacles between transmitter and receiver, which can severely impair the signal. The impact of the obstacles increases with the frequency and signals with very high frequencies cannot penetrate the majority of objects [38]. Therefore, the 60 GHz bands are mainly used for short-range indoors applications. For emphasizing the severe conditions at 60 GHz, consider
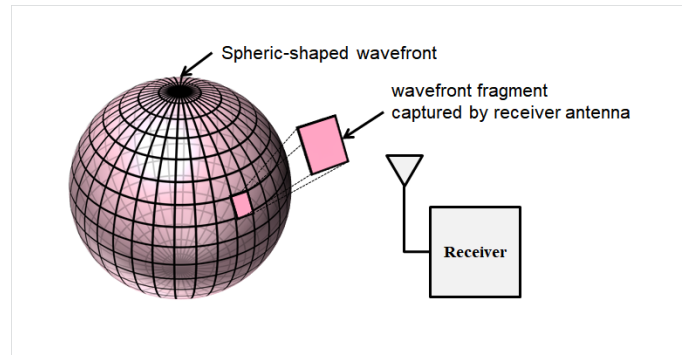


Fig. 1. Model for the FSPL model.

a comparison between 3 GHz and 60 GHz, as depicted in Fig. 2. The signal propagating at 60 GHz suffers an attenuation 25 dB higher than the signal with 3 GHz in the entire evaluated range. Recent developments in digital communication systems, such as high-gain antennas, massive MIMO and beam-forming techniques are being pointed-out as enablers to overcome the high attenuation challenge in outdoors 60 GHz applications.
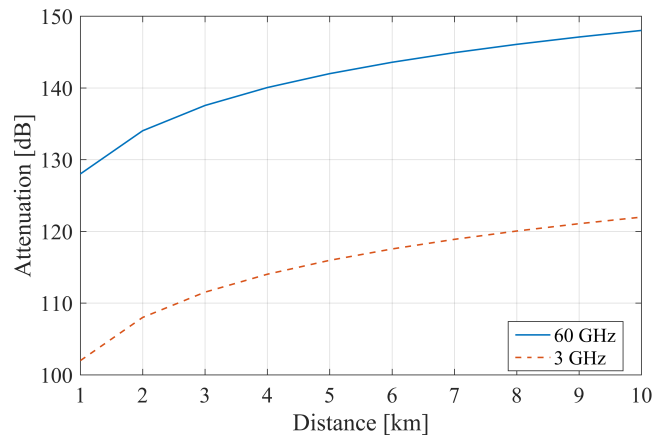


Fig. 2. Free-space loss comparison between signals operating at 3 GHz and 60 GHz.

## B. Rainy Environment

Signals operating at mm-wave frequencies are subjected to rain attenuation. This subsection describes how the rain affects the signal propagation, specifically for frequencies above 10 GHz [39] [40]. The models for estimating the rain attenuation requires a classification of the environment scenario considering its rainfall rate [41]. Table II presents the rain types and the corresponding rainfall rate.

TABLE II
RAIN CLASSIFICATION

| Rain type | Rainfall rate |
|---|---|
| Drizzle | Less than 2.5 mm/h |
| Moderate Rain | More or equal 2.5 mm/h |
| Heavy Rain | Between 10 mm/h and 50 mm/h |
| Violent Rain | More than 50 mm/h |

Based on the rain type defined, it is possible to estimate the average rainfall rate , which leads to the rain coefficient attenuation, given by

$$\gamma_{\mathrm{R}} = p_i R^{\epsilon_i} \tag{4}$$

where $R$ is the rainfall rate. The parameters $p_i$ and $\epsilon_i$ are coefficients that depend on the operating frequency. These coefficients depend also on the polarization of the wave. In this paper, the index $i = 1$ represents the horizontal polarization and the index $i = 2$ represents the vertical polarization. Therefore, $p_1$ and $\epsilon_1$ are the parameters for horizontal polarization and $p_2$ and $\epsilon_2$ are the parameters for vertical polarization. The frequency range used to evaluated $p_i$ and $\epsilon_i$ varies from 1 to 100 GHz [42]. These parameters are are given by

$$\log p_i = \sum_{j=1}^{4} \left( e_i e^{-\left(\frac{\log f - t_i}{g_i}\right)^2} \right) + m_i \log f + d_i$$

$$\epsilon_i = \sum_{j=1}^{5} \left( e_{i+2} e^{-\left(\frac{\log f - t_{i+2}}{g_{i+2}}\right)^2} \right) + m_{i+2} \log f + d_{i+2} \tag{5}$$

Table III shows the constant values for the $p_i$ and $\epsilon_i$ evaluation [38] [43]. The coefficients $e$, $t$, $g$, $m$ and $d$ have been empirically obtained in measurements campaigns and are used to evaluate $p_i$ and $\epsilon_i$. Overall, the Tables present all the coefficients to determine the attenuation caused by the rain, considering both types of polarization, vertical and horizontal. Particularly, for 60 GHz, we have specified the parameters, as presented in Table IV.
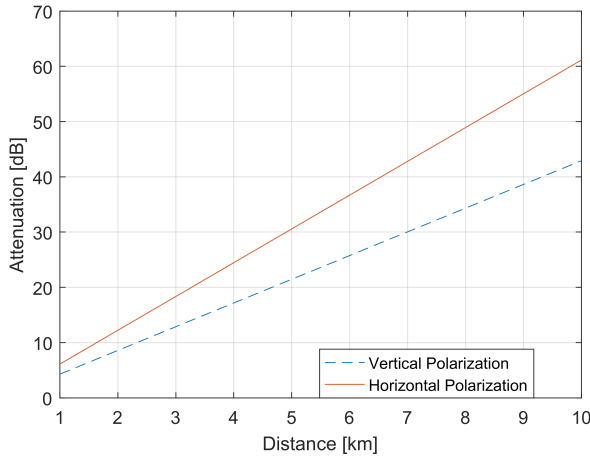


Fig. 3. Comparison between horizontal and vertical polarization.

The antenna polarization plays an important role in the mm-wave signal attenuation in rainy environments. Fig. 3 compares the rain attenuation for vertical and horizontal polarization at 60 GHz, considering the distance range from 1 km to 10 km. It was assumed a rainfall rate of 10 mm/h and the rain parameters for 60 GHz from Table IV.

From Fig. 3 it is possible to notice that the signal with horizontal polarization suffers higher attenuation than the

TABLE III
COEFFICIENTS FOR $p_i$ AND $\epsilon_i$ [43]

| Coefficients for $p_1$ | | | | | |
|---|---|---|---|---|---|
| $j$ | $e_1$ | $t_1$ | $g_1$ | $m_1$ | $d_1$ |
| 1 | -5.33980 | -0.10008 | 1.13098 | -0.18961 | 0.71147 |
| 2 | -0.35351 | 1.26970 | 0.45400 | -0.18961 | 0.71147 |
| 3 | -0.23789 | 0.86036 | 0.15354 | -0.18961 | 0.71147 |
| 4 | -0.94158 | 0.64552 | 0.16817 | -0.18961 | 0.71147 |

| Coefficients for $p_2$ | | | | | |
|---|---|---|---|---|---|
| $j$ | $e_2$ | $t_2$ | $g_2$ | $m_2$ | $d_2$ |
| 1 | -3.80595 | 0.56934 | 0.81061 | 0.16398 | 0.632967 |
| 2 | -3.44965 | -0.22911 | 0.51059 | 0.16398 | 0.632967 |
| 3 | -0.39902 | 0.73042 | 0.11899 | 0.16398 | 0.632967 |
| 4 | 0.50167 | 1.07314 | 0.27195 | 0.16398 | 0.632967 |

| Coefficients for $\epsilon_1$ | | | | | |
|---|---|---|---|---|---|
| $j$ | $e_3$ | $t_3$ | $g_3$ | $m_3$ | $d_3$ |
| 1 | -0.14318 | 1.82442 | -0.55187 | 0.67849 | -1.95537 |
| 2 | 0.29591 | 0.77564 | 0.19822 | 0.67849 | -1.95537 |
| 3 | 0.32177 | 0.63773 | 0.13164 | 0.67849 | -1.95537 |
| 4 | -5.37610 | -0.96230 | 1.47828 | 0.67849 | -1.95537 |
| 5 | 16.1721 | -3.29980 | 3.43990 | 0.67849 | -1.95537 |

| Coefficients for $\epsilon_2$ | | | | | |
|---|---|---|---|---|---|
| $j$ | $e_4$ | $t_4$ | $g_4$ | $m_4$ | $d_4$ |
| 1 | -0.0777 | 2.33840 | -0.76284 | -0.05373 | 0.83433 |
| 2 | 0.5672 | 0.95545 | 0.54039 | -0.05373 | 0.83433 |
| 3 | -0.2023 | 1.14520 | 0.26809 | -0.05373 | 0.83433 |
| 4 | 48.2991 | 0.791669 | 0.116226 | -0.05373 | 0.83433 |
| 5 | 48.5833 | 0.791459 | 0.116479 | -0.05373 | 0.83433 |

TABLE IV
RAIN PARAMETERS FOR 60 GHz FREQUENCY [43]

| | |
|---|---|
| $p_1$ | 0.8606 |
| $p_2$ | 0.7656 |
| $\epsilon_1$ | 0.8515 |
| $\epsilon_2$ | 0.7486 |

signal with vertical polarization. The main reason for this behavior is the non-spherical shape of the raindrops, resulting in higher extension in the to horizontal polarization compared to the vertical one, because of the air resistance [43].

In order to define the overall rain attenuation, it is important to consider the effective rain link, which is the distance between the transmitter and receiver that is affected by the rain. Only effective rain link shall be multiplied by $\gamma_{\mathrm{R}}$ to obtain the overall attenuation introduced by the rain.

### C. Urban Environment

The obstacles in a urban environment, such as buildings, houses, vehicles, lamp posts, human beings, cause reflection, diffraction and scattering in the mm-wave signal. These phenomena result in multipath and attenuation due to fading [44] [45].

Reflection occurs when one electromagnetic wave hits an obstacle with large dimension compared to the signal wavelength. A parcel of the energy is reflected and another one is absorbed by the obstacle. The reflected and absorbed components depends on the incidence angle, material of the obstacle and the operation frequency. The reflected waves can interfere destructively or constructively at the receiver

[44] [46], leading to fading. Fig. 4 shows a representation of an electromagnetic wave propagating from the environment 1 to the environment 2 with incidence angle $\theta_{ti}$, which equals the reflected angle $\theta_r$. The parcel of the wave transmitted to
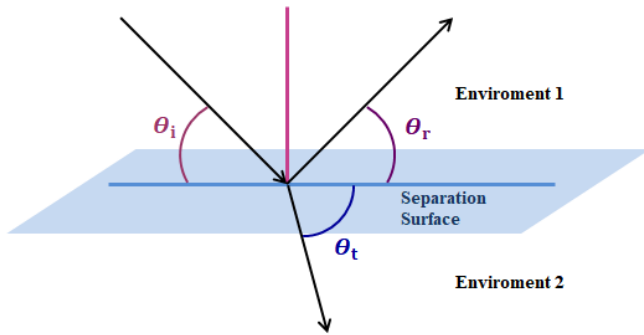


Fig. 4. Model for signal reflection and refraction.

the environment 2 propagates with the transmit angle $\theta_t$. The relationship between the incidence and transmit angles is given by

$$\frac{\cos\theta_t}{\cos\theta_i} = \sqrt{\frac{\mu_1\varepsilon_1}{\mu_2\varepsilon_2}}, \tag{6}$$

where $\mu_i$ is the magnetic permeability and $\varepsilon_i$ is the electrical permittivity of the $i$th environment [38]. The reflection coefficient is given as

$$\Gamma = \frac{\eta_2\mathrm{sen}\theta_i - \eta_1\mathrm{sen}\theta_t}{\eta_2\mathrm{sen}\theta_i + \eta_1\mathrm{sen}\theta_t}, \tag{7}$$

where $\eta_i$ is the intrinsic impedance of the $i$th environment, given by

$$\eta_i = \sqrt{\frac{\mu_i}{\varepsilon_i}}, \tag{8}$$

Scattering occurs when an electromagnetic wave interacts with an irregular shaped object with dimensions smaller than the signal's wavelength [47]. This phenomenon results in several new front waves that propagate in different directions [44].

Diffraction is a phenomenon that occurs when an electromagnetic wave encounters a slit, which is comparable in size to its wavelength. The diffraction level depends on the type of obstacle, wave polarization, operation frequency, signal phase and signal amplitude of the incident wave. The diffracted wave can reach the receiver even in a Non-Line-of-Sight (NLOS) scenario [44] and it can be a propagation mechanism to establish a communication link between a transmitter and a receiver.

The Fresnel field is key to determine the influence of an obstacle in a communication link. The Fresnel field is a set of ellipsoids on the space between transmitter and receiver, in which the two focus of all of ellipsoids are the transmit and receive antennas. The radius of the $n$th Fresnel zone distant $d_1$ meters from the transmitter and $d_2$ meters from the receiver is given by

$$\rho_n = \sqrt{\frac{n\lambda d_1 d_2}{d}}, \tag{9}$$

where $\lambda$ is the wavelength and $d$ is the total link length [38].

The most important Fresnel zone to be considered is the first ellipsoid, which concentrates most of the signal's energy. Fig. 5 illustrates the first Fresnel zone in a communication link.
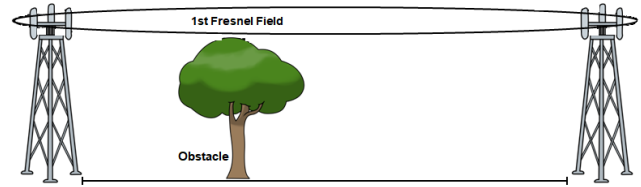


Fig. 5. Fresnel zone between transmitter and receiver.

The obstacles that partially block the first Fresnel zone introduce considerable attenuation in the radio link, which cannot be neglected.

Several models takes reflection, diffraction, refraction, scattering and the interaction with the first Fresnel zone into consideration in order to estimate the attenuation in urban areas.

### D. Vegetation Environment

The morphology of a region also affects the propagation of the mm-wave signals and the vegetation can increase the attenuation of a wireless communication link. This attenuation depends on the vegetation volume and the distance that the signal propagates throughout it [48] [49]. The attenuation caused by foliage obstruction is an important factor to be analyzed in outdoor environments operating in the mm-wave band. The attenuation occurs due to irregular vegetation shapes like uneven oriented trunks, branches, twigs and leaves, resulting in absorption, diffraction and scattering losses in the transmitted signal. Since trees present different shape structures, the study of foliage obstruction is complex [50]. The scenario considered in this paper is illustrated in Fig. 6, where the signal propagates among threes and bushes. Scattering, diffraction and ground reflection are the main characteristics of this environment.
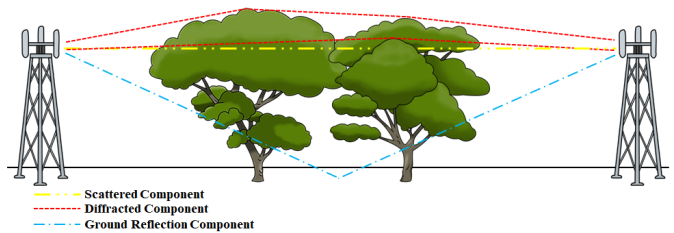


Fig. 6. Signal propagation in a vegetation environment.

The vegetation can introduce a significant attenuation in signals operating in mm-wave bands. The International Telecommunication Union (ITU) recommendation P.833-4 [20] describes an empirical propagation model to estimate the attenuation caused by foliage obstruction as a function of vegetation depth for frequencies raging from 9.6 up to 57.6 GHz. This model estimates the losses caused by scattering, diffraction and reflection introduced by a volume of trees that interacts with

the first Fresnel zone [51]. This model considers the geometry of foliage area illumination, as depicted in Fig. 7.
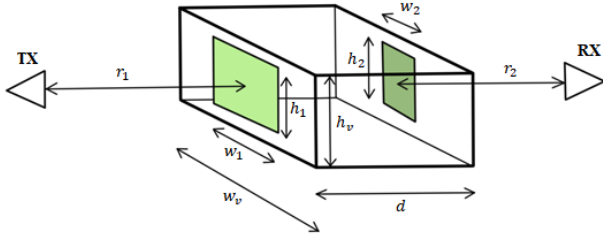


Fig. 7. Geometrical Representation of $A_{\min}$ parameters.

The attenuation introduced by a volume of vegetation with minimal area $A_{\min}$ as a function of the vegetation depth $d$ is given by

$$A_{\text{veg}} = R_\infty d + k \left(1 - e^{\left(-\frac{(R_0 - R_\infty)}{k}\right)} d\right),\tag{10}$$

where

$$R_0 = af\tag{11}$$

and

$$R_\infty = \frac{b}{f^c}\tag{12}$$

The auxiliary variables $a$, $b$ and $c$ are presented in Table V. Frequency $f$ is given in GHz and

$$k = K_0 - 10 \log\left(A_0 \left(1 - e^{\frac{-A_{\min}}{A_0}}\right)\right)\left(1 - e^{-R_f f}\right),\tag{13}$$

with $K_0$, $R_f$ and $A_0$ also presented in Table V. One can note different parameters values depending on the vegetation scenario, in leaf or out of leaf. Such parameters directly impacts the received power, since its expected a high attenuation for in leaf cases.

TABLE V
VEGETATION PARAMETERS [20]

| Parameters | In Leaf | Out of Leaf |
|---|---|---|
| $a$ | 0.2 | 0.16 |
| $b$ | 1.27 | 2.59 |
| $c$ | 0.63 | 0.85 |
| $K_0$ | 6.57 | 12.6 |
| $R_f$ | 0.0002 | 2.1 |
| $A_0$ | 10 | 10 |

The minimum illuminated area $A_{\min}$ represented in Fig. 7 is the product between the minimum width and the minimum height of illuminated vegetation area, leading to [51]

$$A_{\min} = \min(h_1, h_2, h_v) \cdot \min(w_1, w_2, w_v)\tag{14}$$

where the parameters $h_1$, $h_2$, $w_1$ and $w_2$ are described as

$$h_1 = 2r_1 \tan\left(\frac{\varphi_T}{2}\right)\tag{15}$$

$$h_2 = 2r_1 \tan\left(\frac{\varphi_R}{2}\right)\tag{16}$$

$$w_1 = 2r_1 \tan\left(\frac{\phi_T}{2}\right)\tag{17}$$

$$w_2 = 2r_1 \tan\left(\frac{\phi_R}{2}\right)\tag{18}$$

where $\varphi_T$ is the transmit antenna elevation beam-width, $\varphi_R$ is the receive antenna elevation beam-width, $\phi_T$ is transmit antenna azimuth beam-width and $\phi_R$ is the receive antenna azimuth beam-width. Such parameters are illustrated in Fig. 7.

### E. Attenuation Caused by Suspended Particles

Another atmospheric effect that causes attenuation in the mm-wave signal are the oxygen and water vapor absorption, which can play an important role in the total propagation loss for frequencies higher than 10 GHz [52]. Fig. 8 presents this specific attenuation as a function of frequency for dry air and water vapor propagation cases. The first attenuation peak occurs around 22 GHz due to water vapor absorption, and the oxygen absorption introduces an attenuation peak at 60 GHz, compromising the use of this frequency bands for long-range wireless link [9] [24] [29] [53] . On the other hand, the high attenuation at 60 GHz is beneficial for indoor operation and localized hot spots, since this attenuation allows for high reuse factor.
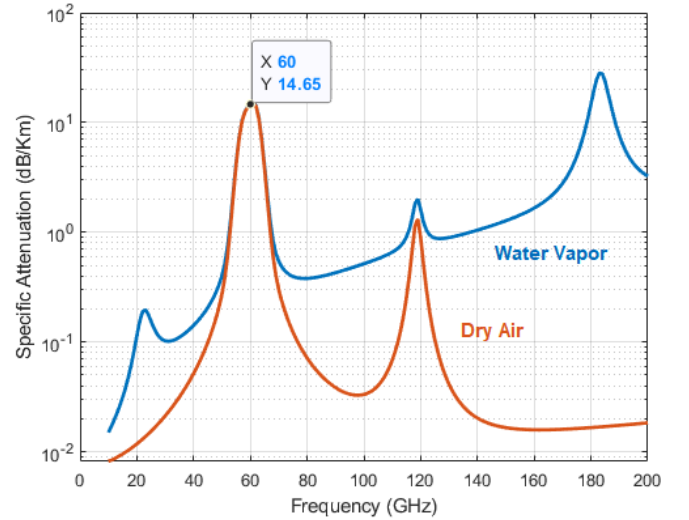


Fig. 8. Attenuation caused by dry air and water vapor as a function of the frequency. Plots obtained using Matlab 5G toolbox based on ITU-R P.676-9 [54]. Used parameter - pressure: 1013 hPa, temperature: $15\,°C$, and density: $7.5$ g/m$^3$.

## III. 5G MODELS FOR PROPAGATION SCENARIOS

The propagation scenario models that can be considered for 5G signals at mm-wave frequencies can be used for estimating the impact of the communication channel, taking the environment peculiarities into consideration. Due to the high signal attenuation in mm-wave range, the propagation models are essential for proper link budget analysis and for proposing countermeasures to overcome the channel limitations. In this section, the most relevant propagation models for 5G signals in mm-wave are presented.

### A. COST 2100 Model

The COST 2100 model is a Geometry-based Stochastic Channel Model (GSCM) [11,55,56] that considers delays by analyzing object geometry in environments that contribute to signal dispersion. The simplified channel is the overlap of different paths due to the interaction between radio waves and objects, which introduces Multipath Components (MPC). The MPCs are characterized by delay, Azimuth of Arrival (AoA), Azimuth of Departure (AoD), Elevation of Arrival (EoA) and Elevation of Departure (EoD) [11]. This channel model is based in clusters that can be classified according with its composition and position in the link [11]. Local clusters are those around the User Equipment (UE) and Base Station (BS), and they have an omnidirectional spread. The far cluster consist of single-bounce and multiple-bounce cluster. The single-bounce clusters are represented by one cluster related to the user and it has an independent delay, allowing it to be mapped to a specific position by combining delay and angles. Multiple-bounce clusters are observed from BS and UEs. The twin clusters are constituted of two clusters related to the BS. One of the clusters defines the angles of arrival at the receiver, and another cluster defines the angles of departure of the MPCs from the transmitter. The circular visibility region is a circular region that determines whether the cluster is active or not for a given user [11]. Overall, the cluster representation enable to analyze the propagation scenarios and the environment impacts [11]. In addition, the COST 2100 can be used for a wide range of frequencies, varying from 0.45 GHz to 100 GHz.

### B. 3GPP TR 38.901 Model

The 3GPP TR 38.901 model is the an extension of the 3GPP TR 38.900 model for frequencies up to 100 GHz. The new model supports UMa, UMi and indoor scenarios. The 3GPP TR 38.901 model can be used for a frequency range from 0.5 to 100 GHz. In the UMi scenario, the model uses a distance away from the $d_{(3D)}$ call that represents the distance between base station height $h_{BS}$ to the height of the mobile station $h_{UE}$. The shadow fading in this model follows the normal distribution with standard deviation equals 4 dB. In order to employ this model, it is necessary to define the environment conditions, such as antenna array used by the devices, the scenario (UMi, UMa, or indoor hotspot (InH)), the frequency and the bandwidth. Also, it is necessary to define if the channel leads to a LOS or NLOS link and the path loss estimation. The model generates the large scale parameters, such as shadow fading and delay propagation. The cluster delay and cluster power are created considering the arrival and departure angles for elevation and azimuth. Finally, the model considers the polarization and random phases and generates the path loss for each cluster [15].

### C. METIS Model

The METIS project provided requirements for 5G networks [57]. In order to evaluate the feasibility of these requirements, the METIS project also proposed a channel model that leads to a propagation environment where several obstacles (buildings, vehicles, houses, threes, people, etc) are considered and the main propagation phenomena (reflection, diffraction, shadowing and scattering) in LOS or NLOS links are taken into account. The models generates propagation matrices of the channel and, which defines the radio channel transfer function [57]. The frequency range for the METIS channel model varies from 0.8 up to 60 GHz for UMi and from 450 MHz up to 6 GHz for UMa. This propagation model can support MIMO and it is widely used as a GSCM [57].

### D. NYUSIM Model

NYUSIM is an open-source channel simulator developed by the New York University based on several measurements campaigns at mm-wave frequencies from 28 to 73 GHz. Different scenarios has been covered: UMa, UMi and rural macrocell. NYUSIM creates sample functions of the spatial and temporal Channel Impulse Responses (CIRs) for directional and omni-directional channel models. It provides an accurate analysis of CIRs in space and time, as well as signal levels. The software is applicable for a wide range of frequencies, varying from 500 MHz up to 100 GHz and bandwidths up to 800 MHz. Ongoing works are being realized to extend the model up to 140 GHz and will be added to the software in future versions [58]. NYUSIM uses the Statistical Spatial Channel Model (SSCM) with time clusters and spatial lobes to model omnidirectional CIR and the AoD and AoA power spectra [59]. The spatial lobes represents main directions of arrival or departure when RF power reaches the receptor over hundreds of nanoseconds. Time clusters are composed from MPCs that propagates with a slight time difference. The NYUSIM software simulator generates several CIR samples for specific distance between the transmitter and the receiver. The number of samples and the distance between the devices are defined by the user. The current NYUSIM software (version 2.0) has 49 input parameters for channel model analysis that are divided into four main categories: channel parameters, antenna properties, spatial consistency parameters and human blockage parameters [60].

### E. mmMAGIC Model

The mmMAGIC project has developed a channel model that is an extension of the WINNER channel model to cover Radio Access Technology (RAT) operating in the frequency range from 6 up to 100 GHz. This model is based on measurement and simulation data. At least 20 measurements campaigns in more than 8 frequency bands have been realized across 5 European countries. The mmMAGIC channel model extends the current GSCMs enabling new features and applications. The major improvements are the addition of blockage effects, ground reflection, building penetration loss, large antenna arrays, wider bandwidths, and provision of spatial consistency. These mmMAGIC features are implemented in Quasi Deterministic Radio Channel Generator (QuaDriGa) 2.0 [61], which is open-source software for channel emulation. The model covers UMi street canyon, UMi open square, indoor shopping mall, indoor office, indoor airport, metro station,

stadium, and outdoor-to-indoor (O2I) environments. Additionally mmMAGIC supports full spatial consistency for a unique moving user terminal, tracking delays, angles, and paths. The mmMAGIC path loss are divided in UMi outdoor LOS, UMi outdoor NLOS, indoor LOS and indoor NLOS [62] [63].

### F. 5GCM Model

The 5GCM is a 5G mm-wave channel model alliance founded by National Institute of Standards and Technology (NIST) with participation of several companies and universities, such as Huawei, Qualcomm and New York University. The scenarios covered by 5GCM are UMi urban street canyon, UMi open-square, outdoor-to-outdoor (O2O), O2I, UMa O2O, UMa O2I and InH. The model is based on 3GPP-3D propagation channel model and the main features are the penetration loss, path loss and blockage for LOS and NLOS scenarios [34].

### G. Models Comparison

In order to compare the path loss among the presented models and a real measurement, a specified a scenario based on the measurements campaign from [64] has been considered as baseline. The measurements have been performed at 73 GHz considering a BS antenna height of 110 m and a UE antenna height of 2 m. Fig. 9 presents the models path loss comparison in the specified scenario, including the measurements from [64].
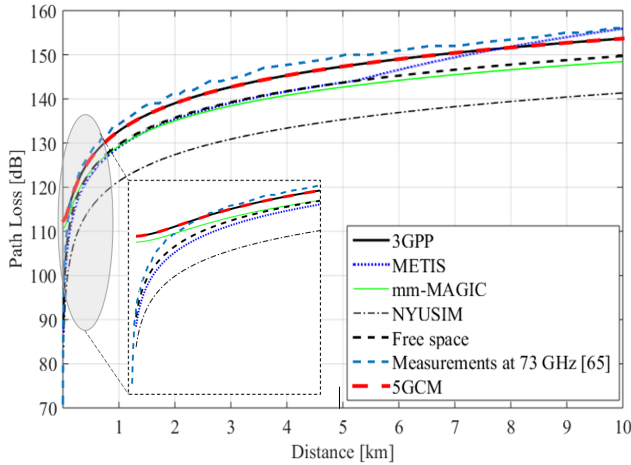


Fig. 9. Path Loss as a function of the distance between transmitter and receiver considering four different channel models in UMi scenario.

From Fig. 9, it is possible to notice that 5GCM and the 3GPP models presents similar slope, which approximate with the measured data in the entire distance range. The METIS and mmMAGIC models presents similar behavior up to 5 km. From this point on, the METIS model estimates a higher attenuation, which comes close to the measurement data for distances larger than 8 km. The breakpoint presented by the METIS model depends on the BS and UE antennas heights and on the operating frequency. One can note the NYUSIM results in an optimistic channel estimation. The main reason for this outcome is that the NYUSIM model only considers the

2D distances in such scenario, which means that the BS and UE antennas heights are not considered. Additionally, a zoom-in-view enables the visualization and models comparison for short distances. One can note that the 3GPP, 5GCM and mm-MAGIC models presented a pessimistic response and not fit well with the experimental data. Table VI summarizes the main features of each model, including the operating frequency, bandwidth, max speed and if the models consider massive MIMO, 3D channels and spatial consistency [65].

### IV. PREDICTION MODELS

This section presents the prediction models for 5G signals. In order to estimate the path loss between transmitter and receiver, it is necessary to parameterize the models according with the environment and channel conditions. There are three kinds of prediction models: the ABG model, the CI free space reference distance model and the CIF model, which is a CI model with a frequency-weighted Path Loss Exponent (PLE) [66] [67]. These models have been studied by the 3GPP standardization group for 5G networks including urban environment, macrocell, microcell, and indoor environments. The frequency range for these prediction models varies from 2 GHz to 73 GHz and the distance range is from 4 m up to 1.238 km. Those models are multi-frequency statistical models that show the large-scale propagation path loss [66] [67]. The following subsections presents the prediction models, their main parameters, and applications.

### A. ABG Prediction Model

The ABG prediction model is an statistical model based on parameters alpha, beta and gamma. These parameters have relationship with the channel models and are used for adjusting the prediction according with the frequency and the distance of the link. The path loss estimation for the ABG model considering one meter as reference is given by

$$P_{\text{Loss}}^{\text{ABG}}(f, d) = 10\alpha \left( \frac{d}{1} \right) + \beta + 10\gamma \log (f) + \chi_\sigma^{\text{ABG}}, \quad (19)$$

where $P_{\text{Loss}}^{\text{ABG}}(f, d)$ is the path loss in dB, $\alpha$ is the coefficient that shows the dependence of path loss with the distance and $\gamma$ represents the dependence on the frequency. $\beta$ is the optimized offset value for the path loss estimation, $d$ is the distance between the transmit and receive antennas, $f$ is the frequency in GHz and $\chi_\sigma^{ABG}$ is a Gaussian random variable with zero mean and standard deviation equals $\sigma$ that describes the signal shadowing [66] [68].

### B. CI Prediction Model

The CI prediction model is a statistical model where the path loss is estimated by

$$P_{\text{Loss}}^{\text{CI}}(f, d) = \text{FSPL}(f, d_0)[dB] + 10n\log \left( \frac{d}{d_0} \right) + \chi_\sigma^{\text{CI}}, \quad (20)$$

where $f$ is the frequency in GHz, $d_0$ is the reference distance in meters, $n$ is the PLE and $\chi_\sigma^{CI}$ is the Gaussian random

TABLE VI
PROPAGATION SCENARIO MODELS COMPARISON

| Channel Model | Frequency Band [GHz] | Bandwidth | Max Speed [km/h] | Massive MIMO | 3D | Spatial Consistency |
|---|---|---|---|---|---|---|
| 3GPP | 6-100 GHz | 10% $f_c$ | - | Yes | Yes | Yes |
| mmMAGIC | 0.5-100 | 100 MHz-2 GHz | 350 | Yes | Yes | Not yet |
| COST | 0.45-100 | - | - | Yes | Yes | Yes |
| 5GCM | 0.5-100 | 2 GHz | 350 | Yes | Yes | Yes |
| METIS | $\leqslant 100$ | 10% $f_c$ | 250 | Yes | Yes | Yes |
| NUYSIM | 0.5-100 | 800 MHz | 108 | Yes | Yes | Yes |

variable with zero mean and standard deviation equals $\sigma$ that represents the signal shadowing [66]. The term $10n$ shows the path loss $d$ meters distant from the transmitter in an environment with PLE $n$. FSPL is given by

$$\text{FSPL}(f, d_0) = 20\log\left(\frac{4\pi f d_0 \times 10^9}{c}\right) \quad (21)$$

*C. CIF Prediction Model*

The CIF prediction model is a statistical model derived from the CI model, where the path loss estimation considering 1 meter as reference is given by

$$P_{\text{Loss}}^{\text{CIF}}(f, d) = \text{FSPL}(f, 1) + \\ + 10n\left(1 + b\left(\frac{f - f_0}{f_0}\right)\right)\log(d) + \chi_\sigma^{CI}. \quad (22)$$

The difference between CIF and CI models is the parameter $b$ in CIF model that represents the linear dependence of the attenuation on the frequency. The $f_0$ is the average frequency, given by

$$f_0 = \frac{\sum_{k=1}^{K} f_k N_k}{\sum_{k=1}^{K} N_k} \quad (23)$$

where $K$ is the number of unique frequencies, $N_k$ is the number of path loss points, which corresponds to the $K$th frequency. It is possible to convert the CIF model to the CI model by making $f_0 = f$ or $b = 0$ [28].

*D. Comparison Between Prediction Models*

The models described in this section have been used to predict the large-scale propagation path loss in different scenarios. These three models are suitable for the frequency range from 2 GHz to 73 GHz for UMa, UMi and InH scenarios [28] [69]. The ABG model presents more parameters in comparison with CI and CIF models. However, the last two models has better performance than the ABG model in terms of stability and prediction accuracy over wide frequency range. This behaviour can be explained by the fact that CI and CIF models use few parameters, including just PLE and $\chi_\sigma^{CI}$, across a wide range of frequencies in comparison with ABG prediction model, which has four parameters: $\alpha$, $\beta$, $\gamma$ and $\chi_\sigma^{ABG}$ [66]. Although ABG model has a higher degree of freedom than CI and CIF models, it is outperformed by the later two in terms of adherence with the measurement data at 60 GHz band [28] [69]. Table

VII summarizes the main scenarios where the ABG model can be used, considering LOS and NLOS cases. Tables VIII and IX present the main scenarios suitable for CI and CIF models, respectively. These tables describes the characteristics of the link applicable for each model assuming UMi, UMa or InH, depending on the frequency range and the link distance. The parameters described in Tables VII, VIII and IX show how the ABG, CI and CIF models are adjusted for the specific scenarios. This parameters were obtained empirically by matching the models to measurement data collected from data campaign.

TABLE VII
SCENARIOS FOR ABG MODEL ASSUMING LOS AND NLOS LINKS [66].

| Scenario | Freq. Range | Dist. Range | $\alpha$ | $\beta$ | $\gamma$ |
|---|---|---|---|---|---|
| UMa LOS | 2-38 GHz | 60-930 m | 1.9 | 35.8 | 1.9 |
| UMi LOS | 28-73 GHz | 27-54 m | 1.1 | 46.8 | 2.1 |
| InH LOS | 2.9-73 GHz | 4-49 m | 1.6 | 32.9 | 1.8 |
| UMa NLOS | 2-38 GHz | 61-1238 m | 3.5 | 13.6 | 2.4 |
| UMi NLOS | 2.9-73 GHz | 48-235 m | 2.8 | 31.4 | 2.7 |
| InH NLOS | 2.9-73 GHz | 4-67 m | 3.9 | 19.0 | 2.1 |

TABLE VIII
SCENARIOS FOR CI MODEL ASSUMING LOS AND NLOS LINKS [66].

| Scenario | Freq. Range | Dist. Range | PLE |
|---|---|---|---|
| UMa LOS | 2-38 GHz | 60-930 m | 2 |
| UMi LOS | 2.9-73 GHz | 27-54 m | 2.1 |
| InH LOS | 2.9-73 GHz | 4-49 m | 3.2 |
| UMa NLOS | 2-38 GHz | 61-1238 m | 2.9 |
| UMi NLOS | 2.9-73 GHz | 48-235 m | 3.2 |
| InH NLOS | 2.9-73 GHz | 4-67 m | 3.1 |

TABLE IX
SCENARIOS FOR CIF MODEL ASSUMING LOS AND NLOS LINKS [66].

| Scenario | Freq. Range | Dist. Range | $n$ | $b$ |
|---|---|---|---|---|
| UMa LOS | 2-38 GHz | 60-930 m | 2.0 | -0.014 |
| UMi LOS | 2.9-73 GHz | 27-54 m | 2.1 | 0.003 |
| InH LOS | 2.9-73 GHz | 4-49 m | 1.5 | -0.102 |
| UMa NLOS | 2-38 GHz | 61-1238 m | 2.9 | -0.002 |
| UMi NLOS | 2.9-73 GHz | 48-235 m | 3.2 | 0.076 |
| InH NLOS | 2.9-73 GHz | 4-67 m | 3.1 | -0.001 |

The prediction models described in this section can be applied for booth indoors and outdoors scenarios. The outdoor scenario can assume a urban environment or rural area with a vegetation morphology with reflection, diffraction and scattering. The indoor scenario covers offices, malls, houses,

etc. The CI and CIF models achieve similar performance for outdoor scenarios and the extra frequency-dependent term in CIF is not necessary in this case [69]. This means that the CI model is the best choice for estimating the path loss in outdoor mm-wave scenarios. CIF and ABG are good options for indoor mm-wave scenarios.

## V. CONNECTION BETWEEN PREDICTION MODELS AND PROPAGATION SCENARIO MODELS

Channel propagation models are used to simulate and reproduce the channel impairments. The main parameters are 2D and 3D distance between transmitter and receiver, environment features, operation frequency and bandwidth. There are several prediction models to estimate the received power considering theses main parameters. However, all of theses models present some specific parameters that links the scenario models with prediction models. For instance, the COST 2100 is based on cluster to represent the channel model and it can be consider an UMi scenario. It is possible to apply all of the prediction models in the cluster to predict the receive power, however, CI and CIF models are more suitable for this application due to the more stable prediction when compared with the ABG prediction model.

The NYUSIM employs the CI model, since the outdoor measurements campaigns do not show any breakpoints in the path loss over the distance between the transmitter and the receiver. NYUSIM employs the 1-$m$ CI model for the entire link instead of CIF or ABG models. The PLE is based on the environment, having value 2 for free space asymptotic two ray ground propagation. Comparing with ABG path loss model used in 3GPP or ITU channel models, the CI model offers better prediction performance for several distances, scenarios and frequencies using fewer parameters.

The 3GPP model uses 3D space between the transmitter and the receiver, taking the BS and UE antennas height into account. Also, it assumes shadow fading distribution to be log-normal with $\sigma = 4$ dB for LOS links. For UMi LOS scenario, this model employs CI path loss model when the 3D distance is smaller than the breakpoint distance. For distances higher than the breakpoint, a new term involving the BS and UE antennas height is included in the CI model. For NLOS UMi street canyon scenario, ABG model is used, and the shadowing fading standard deviation is $\sigma = 7.82$ dB. The 3GPP TR 38.901 UMa LOS path loss model is based on 3GPP TR 36.873 Release 12, for frequencies smaller than 6 GHz, and on TR 38.900 for frequencies higher than 6 GHz. The TR 38.901 omnidirectional path loss models covers frequencies from 0.5 to 100 GHz.

The METIS path loss model employed in UMi scenarios is a modified version of the ITU-R UMi path loss model. Its accuracy is acceptable for frequencies varying from 0.8 up to 60 GHz. METIS breakpoint model is based on sub-6 GHz models, since mm-wave measurements do not report breakpoint. The UMi NLOS path loss model used in METIS is based on 3GPP TR 36.873, which is valid for frequencies up to 6 GHz for Long-Term Evolution (LTE) signals. For UMa scenarios, METIS uses the sub-6 GHz 3GPP TR 36.873. For UMi scenario, METIS uses mm-wave bands to determine the received power using ABG, CI or CIF models.

The 5GCM model employs CI model for for UMi LOS scenario. ABG model could also be used, however the parameter $\alpha$ is similar to the path loss component of the CI model and the parameter $\gamma$ is approximately 2, corresponding to FSPL used in the CI model. 5GCM employs both CI and ABG models for the UMi NLOS scenario. In this case, CI path loss model uses only the PLE, which is defined to minimize the prediction error over the distance between the transmitter and the receiver. The ABG model requires the optimization of three parameters to reduce the prediction error, which implies in a reduction of the shadowing variance when compared with the CI model. Additionally, the 5GCM employs three different UMa path loss models: CI free space reference distance, CIF and ABG. For CI and CIF models, the PLEs are slightly smaller than those used for UMi scenario, which implies in less attenuation over the distance due to higher BS antenna height that reduces the obstructions in the link. The mmMAGIC channel model employs the ABG path loss model for UMi scenarios, similarly to 5GCM. However, the models present a different set of parameters. For instance, mmMAGIC does not support UMa scenarios. The model covers UMi street canyon, UMi open square, indoor shopping mall, indoor office, indoor airport, metro station, stadium, and O2I environments [34] [62].

## VI. CONCLUSION

This tutorial presented key concepts of the emerging 5G wireless systems and the importance of mm-wave to fulfill the requirements of high throughput. Particularly, the 60 GHz band has an important role in the main services of 5G technology such eMBB and URLLC. We demonstrated the main channel propagation challenges, applications and characteristics at 60 GHz, such as path loss, material penetration, foliage and rain attenuation, and others propagation aspects. In this way, channel models are used for simulating and reproducing the propagation channel in a cost-effective way, in order to precisely modeling the channel. We provided a compilation of main mm-wave propagation channel models and recent standards works such COST 2100, NYUSIM, METIS, mmMAGIC, 5GCM and 3GPP TR 38.901, which are obtained by several groups based mainly on ray-tracing methods and extensive measurements campaigns in numerous scenarios and mm-wave bands. Additionally, this tutorial presented the ABG, CI and CIF prediction models and the connection among such models and the propagation scenarios. A path loss comparison between the channel models estimation and a real measurement at 73 GHz has been performed for a urban microcells(UMi). Finally, we provided a comparison between the channel models, focus on the main advantages, differences and limitations for each channel.

## REFERENCES

[1] ITU, "IMT Vision–Framework and overall objectives of the future development of IMT for 2020 and beyond," ITU, Tech. Rep., 2015.

[2] W. Dias, A. Ferreira, R. Kagami, J. S. Ferreira, D. Silva, and L. Mendes, "5G-RANGE: A transceiver for remote areas based on software-defined radio," in *2020 European Conference on Networks and Communications (EuCNC)*, 2020, pp. 100–104, 10.1109/EuCNC48522.2020.9200925.

[3] N. Bhushan, J. Li, D. Malladi, R. Gilmore, D. Brenner, A. Damn-janovic, R. T. Sukhavasi, C. Patel, and S. Geirhofer, "Network densification: the dominant theme for wireless evolution into 5G," *IEEE Communications Magazine*, vol. 52, no. 2, pp. 82–89, 2014, 10.1109/MCOM.2014.6736747.

[4] B. Bertenyi, S. Nagata, H. Kooropaty, X. Zhou, W. Chen, Y. Kim, X. Dai, and X. Xu, "5G NR radio interface," *Journal of ICT Standardization*, vol. 6, no. 1, pp. 31–58, 2018, 10.13052/jicts2245-800X.613.

[5] Z. Pi and F. Khan, "An introduction to millimeter-wave mobile broad-band systems," *IEEE communications magazine*, vol. 49, no. 6, pp. 101–107, 2011, 10.1109/MCOM.2011.5783993.

[6] J. G. Andrews, T. Bai, M. N. Kulkarni, A. Alkhateeb, A. K. Gupta, and R. W. Heath, "Modeling and analyzing millimeter wave cellular systems," *IEEE Transactions on Communications*, vol. 65, no. 1, pp. 403–430, 2016, 10.1109/TCOMM.2016.2618794.

[7] F. Qamar, M. N. Hindia, T. Abbas, K. B. Dimyati, and I. S. Amiri, "Investigation of QoS performance evaluation over 5G network for indoor environment at millimeter wave bands," *International Journal of Electronics and Telecommunications*, vol. 65, no. 1, pp. 95–101, 2019, 10.24425/ijet.2019.126288.

[8] B. Antonescu, M. T. Moayyed, and S. Basagni, "mmWave chan-nel propagation modeling for V2X communication systems," in *2017 IEEE 28th Annual International Symposium on Personal, Indoor, and Mobile Radio Communications (PIMRC)*. IEEE, 2017, pp. 1–6, 10.1109/PIMRC.2017.8292718.

[9] T. S. Rappaport, G. R. MacCartney, M. K. Samimi, and S. Sun, "Wideband Millimeter-Wave Propagation Measurements and Channel Models for Future Wireless Communication System Design," *IEEE Transactions on Communications*, vol. 63, no. 9, pp. 3029–3056, 2015, 10.1109/TCOMM.2015.2434384.

[10] J. Meinilä, P. Kyösti, T. Jämsä, and L. Hentilä, *Radio Technologies and Concepts for IMT-Advanced: WINNER II channel models*, M. Döttling, Ed. Wiley Online Library, 2009, 10.1002/9780470748077.ch3.

[11] L. Liu, C. Oestges, J. Poutanen, K. Haneda, P. Vainikainen, F. Quitin, F. Tufvesson, and P. De Doncker, "The COST 2100 MIMO channel model," *IEEE Wireless Communications*, vol. 19, no. 6, pp. 92–99, 2012, 10.1109/MWC.2012.6393523.

[12] V. Nurmela *et al.*, "Deliverable D1.4: METIS Channel Model," METIS project, Tech. Rep., Sep. 2019. [Online]. Available: https://www.metis2020.com/wp-content/uploads/METIS.

[13] T. S. Rappaport, R. W. Heath Jr, R. C. Daniels, and J. N. Murdock, *Millimeter wave wireless communications*. Pearson Education, 2014.

[14] G. R. Maccartney, T. S. Rappaport, S. Sun, and S. Deng, "Indoor Office Wideband Millimeter-wave Propagation Measurements and Channel Models at 28 and 73 GHz for Ultra-dense 5G Wireless Networks," *IEEE Access*, vol. 3, pp. 2388–2424, 2015, 10.1109/ACCESS.2015.2486778.

[15] I. A. Hemadeh, K. Satyanarayana, M. El-Hajjar, and L. Hanzo, "Millimeter-wave communications: Physical channel models, design considerations, antenna constructions, and link-budget," *IEEE Com-munications Surveys & Tutorials*, vol. 20, no. 2, pp. 870–913, 2017, 10.1109/COMST.2017.2783541.

[16] J. G. Andrews, T. Bai, M. N. Kulkarni, A. Alkhateeb, A. K. Gupta, and R. W. Heath, "Modeling and Analyzing Millimeter Wave Cellular Systems," *IEEE Transactions on Communications*, vol. 65, no. 1, pp. 403–430, 2017, 10.1109/TCOMM.2016.2618794.

[17] H. Zhao, R. Mayzus, S. Sun, M. Samimi, J. K. Schulz, Y. Azar, K. Wang, G. N. Wong, F. Gutierrez, and T. S. Rappaport, "28 GHz millimeter wave cellular communication measurements for reflection and penetration loss in and around buildings in New York city," in *2013 IEEE International Conference on Communications (ICC)*. IEEE, 2013, pp. 5163–5167, 10.1109/ICC.2013.6655403.

[18] S. Deng, G. R. MacCartney, and T. S. Rappaport, "Indoor and outdoor 5G diffraction measurements and models at 10, 20, and 26 GHz," in *2016 IEEE Global Communications Conference (GLOBECOM)*. IEEE, 2016, pp. 1–7, 10.1109/GLOCOM.2016.7841898.

[19] F. Giannetti, M. Luise, and R. Reggiannini, "Mobile and personal com-munications in the 60 GHz band: A survey," *Wireless Personal Commu-nications*, vol. 10, no. 2, pp. 207–243, 1999, 10.1023/A:1018308429332.

[20] ITU, "Recommendation ITU-R P.833-7," ITU, Tech. Rep., Oct 2019. [Online]. Available: http://www.itu.int/rec/R-REC-P.833/en

[21] T. Wu, T. S. Rappaport, and C. M. Collins, "The human body and millimeter-wave wireless communication systems: Interactions and im-plications," in *2015 IEEE International Conference on Communications (ICC)*. IEEE, 2015, pp. 2423–2429, 10.1109/ICC.2015.7248688.

[22] J. S. Lu, D. Steinbach, P. Cabrol, and P. Pietraski, "Modeling human blockers in millimeter wave radio links," *ZTE Communications*, vol. 2012, no. 4, pp. 1164–1179, Jun 2013.

[23] M. R. Akdeniz, Y. Liu, M. K. Samimi, S. Sun, S. Rangan, T. S. Rap-paport, and E. Erkip, "Millimeter wave channel modeling and cellular capacity evaluation," *IEEE journal on selected areas in communications*, vol. 32, no. 6, pp. 1164–1179, 2014, 10.1109/JSAC.2014.2328154.

[24] T. S. Rappaport, G. R. MacCartney, M. K. Samimi, and S. Sun, "Wideband Millimeter-Wave Propagation Measurements and Channel Models for Future Wireless Communication System Design," *IEEE transactions on Communications*, vol. 63, no. 9, pp. 3029–3056, 2015, 10.1109/TCOMM.2015.2434384.

[25] A. Alkhateeb, G. Leus, and R. W. Heath, "Compressed sensing based multi-user millimeter wave systems: How many measurements are needed?" in *2015 IEEE International Conference on Acoustics, Speech and Signal Processing (ICASSP)*. IEEE, 2015, pp. 2909–2913, 10.1109/ICASSP.2015.7178503.

[26] J. F. Buckwalter, S. Daneshgar, J. Jayamon, and P. Asbeck, "Series power combining: Enabling techniques for Si/SiGe millimeter-wave power amplifiers," in *2016 IEEE 16th Topical Meeting on Silicon Monolithic Integrated Circuits in RF Systems (SiRF)*. IEEE, 2016, pp. 116–119, 10.1109/SIRF.2016.7445485.

[27] F. E. Mahmouli and S. D. Walker, "4-Gbps uncompressed video trans-mission over a 60-GHz orbital angular momentum wireless channel," *IEEE Wireless Communications Letters*, vol. 2, no. 2, pp. 223–226, 2013, 10.1109/WCL.2013.012513.120686.

[28] S. Sun, T. S. Rappaport, S. Rangan, T. A. Thomas, A. Ghosh, I. Z. Kovacs, I. Rodriguez, O. Koymen, A. Partyka, and J. Jarvelainen, "Propagation path loss models for 5G urban micro-and macro-cellular scenarios," in *2016 IEEE 83rd Vehicular Technology Conference (VTC Spring)*. IEEE, 2016, pp. 1–6, 10.1109/VTCSpring.2016.7504435.

[29] T. Yilmaz, E. Fadel, and O. B. Akan, "Employing 60 GHz ISM band for 5G wireless communications," in *2014 IEEE international black sea conference on communications and networking (BlackSeaCom)*. IEEE, 2014, pp. 77–82, 10.1109/BlackSeaCom.2014.6849009.

[30] H. Singh, R. Prasad, and B. Bonev, "The Studies of Millimeter Waves at 60 GHz in Outdoor Environments for IMT Applications: A State of Art," *Wireless Personal Communications*, vol. 100, no. 2, pp. 463–474, 2018, doi.org/10.1007/s11277-017-5090-6.

[31] F. Schwering and A. A. Oliner, "Millimeter-wave antennas," in *Antenna Handbook*. Springer, 1988, pp. 1135–1282.

[32] R. J. Weiler, M. Peter, W. Keusgen, E. Calvanese-Strinati, A. De Domenico, I. Filippini, A. Capone, I. Siaud, A.-M. Ulmer-Moll, A. Maltsev *et al.*, "Enabling 5G backhaul and access with millimeter-waves," in *2014 European Conference on Networks and Communications (EuCNC)*. IEEE, 2014, pp. 1–5, 10.1109/EuCNC.2014.6882644.

[33] N. Guo, R. C. Qiu, S. S. Mo, and K. Takahashi, "60-GHz millimeter-wave radio: Principle, technology, and new results," *EURASIP journal on Wireless Communications and Networking*, vol. 2007, no. 1, pp. 48–48, 2007, 10.1155/2007/68253.

[34] T. S. Rappaport, Y. Xing, G. R. MacCartney, A. F. Molisch, E. Mellios, and J. Zhang, "Overview of Millimeter Wave Communications for Fifth-Generation (5G) Wireless Networks—With a Focus on Propagation Models," *IEEE Transactions on Antennas and Propagation*, vol. 65, no. 12, pp. 6213–6230, 2017, 10.1109/TAP.2017.2734243.

[35] L. L. Yang, "60 GHz: opportunity for gigabit WPAN and WLAN con-vergence," *ACM SIGCOMM Computer Communication Review*, vol. 39, no. 1, pp. 56–61, 2008, doi.org/10.1145/1496091.1496101.

[36] A. KATO, K. SATO, M. FUJISE, and S. KAWAKAMI, "Propagation characteristics of 60-GHz millimeter waves for ITS inter-vehicle com-munications," *IEICE transactions on communications*, vol. 84, no. 9, pp. 2530–2539, 2001.

[37] M. Kamarudin, Y. Nechayev, and P. Hall, "Performance of antennas in the on-body environment," in *2005 IEEE Antennas and Propagation Society International Symposium*, vol. 3. IEEE, 2005, pp. 475–478, 10.1109/APS.2005.1552290.

[38] J. A. J. Ribeiro, *Propagação das ondas eletromagnéticas: princípios e aplicações*. Érica, 2004.

[39] F. Moupfouma, "Electromagnetic waves attenuation due to rain: A pre-diction model for terrestrial or LOS SHF and EHF radio communication links," *Journal of Infrared, Millimeter, and Terahertz Waves*, vol. 30, no. 6, pp. 622–632, 2009, doi.org/10.1007/s10762-009-9481-y.

[40] D. Hogg, "Path diversity in propagation of millimeter waves through rain," *IEEE Transactions on Antennas and Propagation*, vol. 15, no. 3, pp. 410–415, 1967, 10.1109/TAP.1967.1138919.

[41] L. Zhao, L. Zhao, Q. Song, C. Zhao, and B. Li, "Rain Attenuation Prediction Models of 60 GHz Based on Neural Network and Least Squares-Support Vector Machine," in *The Proceedings of the Second*

*International Conference on Communications, Signal Processing, and Systems.* Springer, 2014, pp. 413–421, 10.1007/978-3-319-00536-2_48.

[42] J. Sander, "Rain attenuation of millimeter waves at $\lambda$= 5.77, 3.3, and 2 mm," *IEEE Transactions on Antennas and Propagation*, vol. 23, no. 2, pp. 213–220, 1975, 10.1109/TAP.1975.1141059.

[43] ITU, "Specific attenuation model for rain for use in prediction methods," ITU, Recommendation ITU-R P.838-3, Tech. Rep., 2005.

[44] M. M. Ahamed and S. Faruque, "Propagation Factors Affecting the Performance of 5G Millimeter Wave Radio Channel," in *2016 IEEE International Conference on Electro Information Technology (EIT)*. IEEE, 2016, pp. 0728–0733, 10.1109/EIT.2016.7535329.

[45] A. Yamamoto, K. Ogawa, T. Horimatsu, A. Kato, and M. Fujise, "Path-loss prediction models for intervehicle communication at 60 GHz," *IEEE Transactions on vehicular technology*, vol. 57, no. 1, pp. 65–78, 2008, 10.1109/TVT.2007.901890.

[46] G. S. Murty, "Reflection, transmission and attenuation of elastic waves at a loosely-bonded interface of two half spaces," *Geophysical Journal International*, vol. 44, no. 2, pp. 389–404, 1976, 10.1111/j.1365-246X.1976.tb03663.x.

[47] J. A. Ogilvy and H. M. Merklinger, *Theory of wave scattering from random rough surfaces*. ASA, 1991.

[48] M. Cheffena and T. Ekman, "Modeling the dynamic effects of vegetation on radiowave propagation," in *2008 IEEE International Conference on Communications*. IEEE, 2008, pp. 4466–4471, 10.1109/ICC.2008.838.

[49] A. I. Sulyman, H. Seleem, A. Alwarafy, K. M. Humadi, and A. Alsanie, "Effects of Solar Radio Emissions on Outdoor Propagation Path Loss Models at 60 GHz bands for Access/backhaul links and D2D communications," *IEEE Transactions on Antennas and Propagation*, vol. 65, no. 12, pp. 6624–6635, 2017, 10.1109/TAP.2017.2759959.

[50] A. Seville and K. Craig, "Semi-empirical model for millimetre-wave vegetation attenuation rates," *Electronics letters*, vol. 31, no. 17, pp. 1507–1508, 1995.

[51] D. Didascalou, M. Younis, and W. Wiesbeck, "Millimeter-wave scattering and penetration in isolated vegetation structures," *IEEE transactions on geoscience and remote sensing*, vol. 38, no. 5, pp. 2106–2113, 2000, 10.1109/36.868869.

[52] M. Williamson, G. Athanasiadou, and A. Nix, "Investigating the effects of antenna directivity on wireless indoor communication at 60 GHz," in *Proceedings of 8th International Symposium on Personal, Indoor and Mobile Radio Communications-PIMRC'97*, vol. 2. IEEE, 1997, pp. 635–639, 10.1109/PIMRC.1997.631109.

[53] P. Rosenkranz, "Shape of the 5 mm oxygen band in the atmosphere," *IEEE Transactions on Antennas and Propagation*, vol. 23, no. 4, pp. 498–506, 1975, 10.1109/TAP.1975.1141119.

[54] ITU, "Recommendation ITU-R P.676-9: Attenuation by atmospheric gases," ITU-R, Tech. Rep., 2012.

[55] K. Haneda *et al.*, "5G 3GPP-Like Channel Models for Outdoor Urban Microcellular and Macrocellular Environments," in *2016 IEEE 83rd Vehicular Technology Conference (VTC Spring)*, 2016, pp. 1–7, 10.1109/VTCSpring.2016.7503971.

[56] K. Haneda, L. Tian, H. Asplund, J. Li, Y. Wang, D. Steer, C. Li, T. Balercia, S. Lee, Y. Kim *et al.*, "Indoor 5G 3GPP-like channel models for office and shopping mall environments," in *2016 IEEE International Conference on Communications Workshops (ICC)*. IEEE, 2016, pp. 694–699, 10.1109/ICCW.2016.7503868.

[57] J. Medbo *et al.*, "Channel Modelling for the Fifth Generation Mobile Communications," in *The 8th European Conference on Antennas and Propagation (EuCAP 2014)*. IEEE, 2014, pp. 219–223, 10.1109/EuCAP.2014.6901730.

[58] Y. Xing and T. S. Rappaport, "Propagation measurement system and approach at 140 GHz-moving to 6G and above 100 GHz," in *2018 IEEE Global Communications Conference (GLOBECOM)*. IEEE, 2018, pp. 1–6, 10.1109/GLOCOM.2018.8647921.

[59] M. K. Samimi and T. S. Rappaport, "3-D millimeter-wave statistical channel model for 5G wireless system design," *IEEE Transactions on Microwave Theory and Techniques*, vol. 64, no. 7, pp. 2207–2225, 2016, 10.1109/TMTT.2016.2574851.

[60] NYU WIRELESS. (2019, Oct) NYUSIM Version 2.0 Now Available. Accessed on Dec. 2020. [Online]. Available: https://wireless.engineering.nyu.edu/nyusim/

[61] S. Jaeckel, L. Raschkowski, K. Börner, and L. Thiele, "Quadriga: A 3-d multi-cell channel model with time evolution for enabling virtual field trials," *IEEE Transactions on Antennas and Propagation*, vol. 62, no. 6, pp. 3242–3256, 2014, 10.1109/TAP.2014.2310220.

[62] G. I. P. P. Partnership. mmMAGIC: Millimetre-Wave Based Mobile Radio Access Network for Fifth Generation Integrated Communications. Sep 2019. [Online]. Available: https://5g-ppp.eu/mmmagic/

[63] M. Peter *et al.*, "Measurement results and final mmMAGIC channel models," mmMAGIC project, Tech. Rep., 2017, Deliverable 2.

[64] G. R. MacCartney and T. S. Rappaport, "Rural Macrocell Path Loss Models for Millimeter Wave Wireless Communications," *IEEE Journal on Selected Areas in Communications*, vol. 35, no. 7, pp. 1663–1677, 2017, 10.1109/JSAC.2017.2699359.

[65] S. Servigne, T. Ubeda, A. Puricelli, and R. Laurini, "A methodology for spatial consistency improvement of geographic databases," *GeoInformatica*, vol. 4, no. 1, pp. 7–34, 2000, 10.1023/A:1009824308542.

[66] S. Sun, T. S. Rappaport, T. A. Thomas, A. Ghosh, H. C. Nguyen, I. Z. Kovács, I. Rodriguez, O. Koymen, and A. Partyka, "Investigation of prediction accuracy, sensitivity, and parameter stability of large-scale propagation path loss models for 5G wireless communications," *IEEE Transactions on Vehicular Technology*, vol. 65, no. 5, pp. 2843–2860, 2016, 10.1109/TVT.2016.2543139.

[67] A. I. Sulyman, A. Alwarafy, G. R. MacCartney, T. S. Rappaport, and A. Alsanie, "Directional radio propagation path loss models for millimeter-wave wireless networks in the 28-, 60-, and 73-GHz bands," *IEEE Transactions on Wireless Communications*, vol. 15, no. 10, pp. 6939–6947, 2016, 10.1109/TWC.2016.2594067.

[68] N. Rupasinghe, Y. Kakishima, and I. Güvenç, "System-level performance of mmWave cellular networks for urban micro environments," in *2017 XXXIInd General Assembly and Scientific Symposium of the International Union of Radio Science (URSI GASS)*. IEEE, 2017, pp. 1–4, 10.23919/URSIGASS.2017.8105388.

[69] S. Sun, G. R. MacCartney, and T. S. Rappaport, "Millimeter-wave distance-dependent large-scale propagation measurements and path loss models for outdoor and indoor 5G systems," in *2016 10th European Conference on Antennas and Propagation (EuCAP)*. IEEE, 2016, pp. 1–5, 10.1109/EuCAP.2016.7481506.

**Gustavo Kreuzer Marengo** received the B.Sc. degrees from Inatel, Brazil, in 2018, in telecommunication engineering. He has worked at Rosenberger company from 2018 to July 2019. Since August 2019, he has been a Master student from Inatel in telecommunication and RF with focus on Artificial Intelligence and Machine Learning research area.

**Eduardo Saia Lima** received his B.Sc. and M.Sc. degrees from Inatel, Brazil, in 2017 and 2019, respectively and is a PhD student in Telecommunication in the same institution. Has experience in teaching for being a tutor in electronic circuits, digital electronics and optics communications on undergraduate courses from Inatel from 2017 to 2019 in the Teaching Internship Program (PED). Currently acts as researcher for the Wireless and Optical Convergent Access (WOCA) Laboratory at Inatel.

**Gabriel Eduardo Silva Leite** received the B.Sc. degrees from Inatel, Brazil, in 2017, in telecommunication engineering.He has worked at Digital Antena company in 2017 and Neomera company in 2018. Since August 2019, he has been a Master student from Inatel in telecommunication are with focus digital transmission of signals.

**Arismar Cerqueira Sodré Junior** received the B.Sc. degree in electrical engineering from the Federal University of Bahia, Brazil, in 2001, the M.Sc. degree from the State University of Campinas (Unicamp), Brazil, in 2002, and the Ph.D. degree from Scuola Superiore Sant'Anna, Italy, in 2006. He was an Invited Researcher and Professor from many world-recognized universities, such as the University of Oulu (2017), Scuola Superiore Sant'Anna, Italy (from 2015 to 2019), Danish Technical University, Denmark (2013), Max-Planck Institute, Germany (2010), and University of Bath, U.K. (2004, 2005 and 2007). He was an Associate Professor with the Unicamp from March 2009 to August 2011, when he joined the National Institute of Telecommunications, Brazil, to work in the same position. Since 2009, he has been acting as a Coordinator of R&D Projects on diverse areas of telecommunications, including antennas, 5G networks, radars and microwave photonics. He is a holder of 10 patents, has transferred 24 products to the industry, and has published 241 scientific papers.

**Luciano Leonel Mendes** received the B.Sc. and M.Sc. degrees from Inatel, Brazil, in 2001 and 2003, respectively, and the Doctor degree from Unicamp, Brazil, in 2007, all in electrical engineering. Since 2001, he has been a Professor with Inatel, where he has acted as the Technical Manager of the Hardware Development Laboratory from 2006 to 2012. From 2013 to 2015, he was a Visiting Researcher with the Technical University of Dresden in the Vodafone Chair Mobile Communications Systems, where he has developed his postdoctoral. In 2017, he was elected Research Coordinator of the 5G Brazil Project, an association involving industries, telecom operators, and academia which aims for funding and build an ecosystem toward 5G, improving the discussions about the Brazilian needs for this network and how Brazil can contribute with the international standardization.